Title: Novel Automatic Method for the Fusion of ALS and TLS LiDAR Data for Robust Assessment of Tree Crown Structure

This paper appears in: IEEE Transactions on Geoscience and Remote Sensing

Date of Publication: 2017

Author(s): Claudia Paris, David Kelbe, Jan van Aardt, Lorenzo Bruzzone,

Volume:

Page(s):

DOI:10.1109/TGRS.2017.2675963

A Novel Automatic Method for the Fusion of ALS and TLS LiDAR Data for Robust Assessment of Tree Crown Structure

Claudia Paris, Student Member, *IEEE*, David Kelbe, Jan van Aardt, and Lorenzo Bruzzone, Fellow, *IEEE*

***Abstract*— Tree crown structural parameters are key inputs to studies spanning forest fire propagation, invasive species dynamics, avian habitat provision, and so on, but these parameters consistently are difficult to measure. While airborne laser scanning (ALS) provides uniform data and a consistent nadir perspective necessary for crown segmentation, the data characteristics of terrestrial laser scanning (TLS) make such crown segmentation efforts much more challenging. We present a data fusion approach to extract crown structure from TLS, by exploiting the complementary perspective of ALS. Multiple TLS point clouds are automatically registered to a single ALS point cloud by maximizing the normalized cross correlation between the global ALS canopy height model (CHM) and each of the local TLS CHMs through parameter optimization of a planar Euclidean transform. Per-tree canopy segmentation boundaries, which are reliably obtained from ALS, can then be adapted onto the more irregular TLS data. This is repeated for each TLS scan; the combined segmentation results from each registered TLS scan and the ALS data are fused into a single per-tree point cloud, from which canopy-level structural parameters readily can be extracted.**

***Index Terms*— Airborne laser scanning (ALS), forest structure, forestry, light detection and ranging (LiDAR), registration, remote sensing, terrestrial laser scanning (TLS).**

I. Introduction

TREE canopy structure is defined as the spatial organization of the above-ground components of vegetation [1], and encompasses information about the position, quantity, type, and connectivity of both the foliage and supporting woody components [2]. While stand-level parameters provide relatively simple metrics over large areas, it is often of interest to understand object-level tree structure, for example, of the individual tree crowns, which comprise the forest canopy. Here, we distinguish an important note of scale and focus our review on the assessment of individual tree crowns, as opposed to the overarching forest canopies.

Tree crowns have important implications to wild land fire dynamics [3], [4] avian habitat provision [5], [6], microclimates [6], and estimation of the fractal dimension of trees [7]. Within a tree crown, the net leaf surface area drives the size of the plant-atmosphere interface, which affects the rate and balance of biotic exchanges through photosynthesis and transpiration [8]. Likewise, the distribution of individual elements (e.g., leaves and branches) governs radiation penetration through to lower-canopy strata [9]–[11], with implications for forest growth and productivity [12], [13]. Accurate and precise measurement of crown structure is, therefore, an enviable goal for systematic characterization and modeling of forest productivity and related dynamics.

However, explicit measurement of tree crowns using conventional techniques is complicated, due to the complex structure of irregular, natural surfaces. Despite a long history of forest mensuration, traditional methods for quantifying canopy structure remain limited in their ability to enable detailed, quantitative, and spatially explicit measurements [6], [14]. As a result, tree-level parameters are often restricted to coarse metrics, such as crown height, crown base height, and crown width, while more informative metrics are modeled based on lower level parameters [15]. Crown volume, in particular, has been reported as one of the more difficult parameters to obtain [16]. Traditional techniques rely on allometric equations to parameterize geometric primitives (e.g., cones and ellipsoids) and require species information and certain field-measured variables [15].

In contrast, laser scanning records range data based on an emitted laser pulse [17], thus providing nondestructive, high-resolution, and repeatable 3-D surveys of individual tree crowns. Laser scanning has a demonstrated capability to address the limitations of traditional measurement approaches [18], both from airborne and terrestrial platforms. Airborne laser scanning (ALS) utilizes an across-track scanning mechanism, in conjunction with along-track aircraft movement [19], in order to sample a wide-area swath below the aircraft. While large-footprint sensors have focused on stand-scale parameters, e.g., mean canopy height [20], increasingly fine footprints (submeter) and point densities (>15 hits/m^2) [21] have enabled the detection and measurement of individual tree canopy parameters, including crown volume.

A common approach to ALS-based crown measurement is to fit assumed geometric shapes to light detection and ranging (LiDAR) point clouds [22], in order to derive basic tree crown parameters [23]–[27]. However, these methods rely on a priori species identification for parameterizing the appropriate geometric crown shape, information that is often unavailable from remote sensing data [16]. This is especially challenging for heterogeneous nonmanaged forest environments. Moreover, these simple geometric models are coarse when compared to the fidelity of ALS measurements. We, therefore, argue that due to the recent trend towards higher point density LiDAR collection, direct measurement of tree crowns should be

considered [16].

Several alternative approaches have been pursued for ALS, based on either graph-based segmentation or direct measurement. In [28] the authors used normalized cut segmentation to detect individual trees, including those below canopy, theoretically allowing for direct computation of volume, even though quantitative results were not presented. Similarly, in [29] the authors employed a graph-based segmentation algorithm with potential for crown volume assessment based on existing techniques. On the other hand, in [16], the authors developed a direct, wrapped surface reconstruction technique based on radial basis functions. Irregular tree crown shapes were validated using survey-grade equipment to assess goodness-of-fit. Among other reported metrics, the authors modeled crown volume at an $R^2 = 0.84/0.89$ for coniferous/deciduous trees. Finally, [22] used computational geometry to measure explicit crown volume using 3-D alpha shapes and convex hulls. These estimates were validated against field-measured values and modeled ellipsoids, with R^2=0.83 (best), but significant underestimation (-24%, on average), attributed to insufficient LiDAR returns from the lower crown regions.

The observed challenges in crown volume assessment with ALS [30] underscore several fundamental system limitations of ALS. A first limitation is the reduced capability to sample sub-canopy structure. Discrete-return ALS, for example, records only the first and last, or perhaps a few, e.g., up to five, backscattered returns for each emitted laser pulse. As a result, limited information from the inner or lower canopy is obtained [18], [31]. While waveform-digitizing LiDAR [32] offers potential to rectify this gap, the systems are still poorly understood, and there remains a measurement gap due to dead time in the temporal digitization of the return pulse. A second limitation is related to measurement characteristics: as a result of limited incidence angles constrained to predominantly nadir, and finite footprint sizes on the order of 0.1-0.5 m, ALS may be unable to detect small canopy gaps [6], [33], [34], or other fine-scale structures. Finally, when acquired with low laser sampling density, these data do not allow for a comprehensive representation of the crown structure.

Recent studies have hinted at the potential to address these concerns via fusion with a complementary upward-looking laser ranging system, i.e., terrestrial laser scanning (TLS) [35]. TLS provides hemispherical scanning from a ground-based platform, and thus samples different parts of the forest structure. In [31] the authors examined the voxel column percentile distributions of point returns for both ALS and TLS and demonstrated that a higher percentage of laser pulses intercepts the top of the canopy for ALS, with limited returns within the canopy and understory. Likewise, TLS exhibited a higher number of returns from the lower canopy, but had fewer returns in the upper canopy. This complementarity has prompted a growing interest in utilizing TLS to complement the strengths of ALS [36], [37], and thus link ground-level structural measurements with the synoptic perspective of ALS.

However, there has been limited research in this area, in part due to the difficult prerequisite of registration [38]–[42]. Even for TLS acquisition, a primary limitation is the need to position reference targets to register the multiangular scans, which often requires time-consuming manual refinements, although marker-free techniques have been developed [38],[43]. However, ALS data, which provide uniform sampling of the upper canopy surface, may provide the necessary linkage for registration of TLS and ALS data. In this paper, we propose a novel and automatic method for the fusion of ALS and TLS LiDAR data in open woodland forest toward a more comprehensive and robust assessment of the tree crown structure. By exploiting the synoptic perspective of ALS and TLS data, we obtain a more comprehensive representation of the crown structure by automatically registering and segmenting the TLS data via the proxy of ALS data. The main objectives of this work are to: 1) employ the ALS to automatically register and segment multiple TLS and 2) integrate the 3-D LiDAR point clouds of both the ALS and TLS data for quantitative measurements of tree crown structure.

The paper is organized as follows. Section II presents the architecture of the proposed data fusion approach and describes all the phases of the method in detail. Section III illustrates the considered data set by presenting the study area, the TLS measurement setup, and the ALS data. Section IV presents the obtained experimental results, and Section V provides the conclusion and outlook.

II. Proposed Approach

In this paper, we present a novel approach to exploit the complementary LiDAR data coverage acquired from different viewpoint perspectives, specifically ALS and TLS, in order to accurately characterize 3-D structure of individual tree crowns. The proposed method is separated into three main phases: 1) preprocessing; 2) segmentation of the TLS data, driven by the ALS segmentation results; and 3) automatic registration and fusion of ALS and TLS LiDAR scans. Fig. 1 shows the block scheme of the proposed data fusion method. In the following, we describe in detail each phase of the proposed method.

A. Preprocessing

The first phase, *preprocessing*, seeks to extract rasterized canopy height models (CHMs) from the airborne and terrestrial LiDAR data, in addition to a crown segmentation image, S_a, obtained from the ALS data. Assume N evenly distributed terrestrial point clouds and a single ALS point cloud acquired over the same area. Each point cloud is first normalized by the ground elevation (extracted from each point cloud), such that the z coordinate now represents the height above ground for that x-y coordinate. Let $P_{t,1} \dots P_{t,n} \dots . P_{t,N}$ be the normalized terrestrial point clouds, and let P_a be the normalized airborne point cloud. Then, rasterized CHMs (I_a and $I_{t,1} \dots I_{t,n} \dots . I_{t,N}$ for the airborne and terrestrial data, respectively) are generated by gridding the highest point within each cell. The next step is to

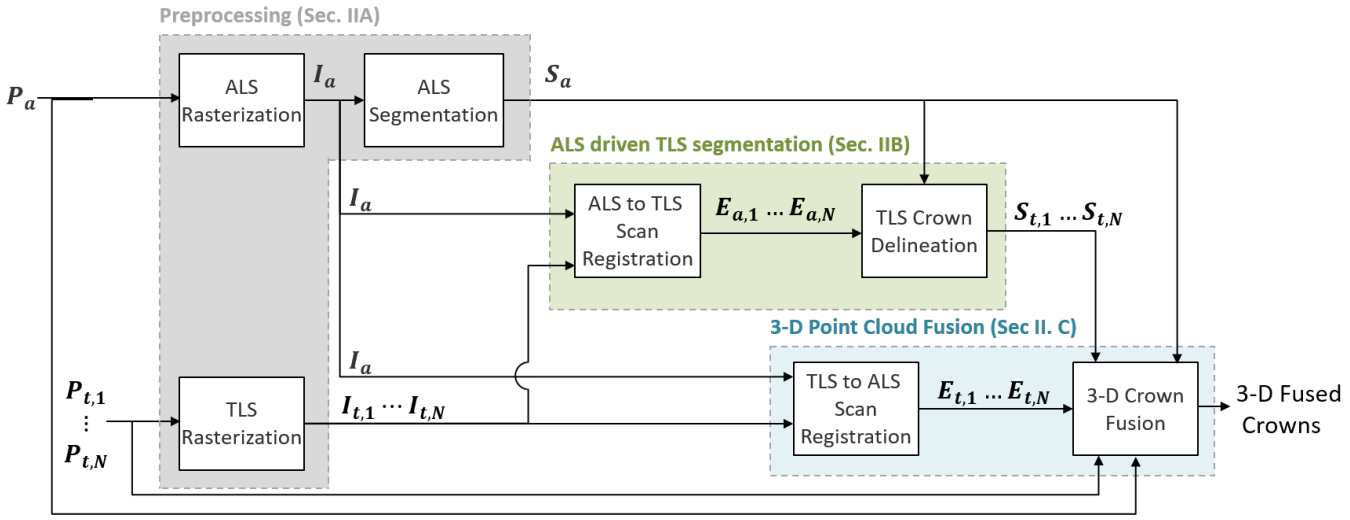

Fig. 1. Block scheme of the proposed data fusion approach to the accurate reconstruction of the 3-D structure of the crown. The three main phases of the method are highlighted in bright colors. The TLS point clouds, $P_{t,1} \dots P_{t,n} \dots . P_{t,N}$, and the ALS point cloud, P_a, are preprocessed to generate the CHMs, $I_{t,1} \dots I_{t,n} \dots . I_{t,N}$ and I_a, respectively, and the segmented ALS image, S_a. First, the ALS is registered to the TLS scan to segment the single tree crowns in the terrestrial data, i.e., $S_{t,1} \dots S_{t,n} \dots . S_{t,N}$. Then, the method registers the TLS scans the ALS data to fuse the segmented crown in the 3-D point cloud.

extract a segmentation image, S_a, representing the set of tree crowns, obtained from the ALS data. Because of the comprehensive, uniform sampling of the upper canopy structure, provided by the airborne acquisition (ALS), the detection and the delineation of the individual tree crowns are performed based only on the airborne LiDAR data. Since we aim to assess the effectiveness of fusing ALS and TLS data, in the considered implementation, the crowns were manually delineated on the ALS CHM. However, any automatic segmentation method can be employed to delineate the individual tree crowns [44]-[48].

The obtained segmentation result is used to drive the segmentation onto the TLS CHMs, after appropriate registration of the ALS data to TLS scans (second stage; Section II-B). At the end of this stage, the segmented crowns are registered into a common coordinate system and fused directly to the 3-D point cloud space (third stage; Section II-C).

B. ALS-Driven TLS Segmentation

The second stage, *TLS Segmentation*, seeks to automatically delineate the crown boundaries in the TLS scans by taking advantage of the ALS data characteristics. Note that TLS data usually require time-consuming manual canopy segmentation, based on visual inspection of the 3-D LiDAR data, due to the side-view scanning, which typically does not measure the horizontal structure of the forest [44]. Few studies have focused on individual tree segmentation using TLS [49],[50]; moreover, the majority of studies have conducted experiments for urban forests characterized by almost no canopy overlap [51],[52].

We adapt the segmentation result, S_a, obtained from the airborne data (see Section II-A) and apply it to the TLS data to accurately delineate the crown boundaries visible in the terrestrial scans, thereby taking advantage of the availability of the ALS data. In other words, because of the comprehensive sampling of the upper canopy from a nadir perspective, the ALS segmentation result is more accurate than any result automatically obtained from TLS data. To leverage this complementarity, spatial alignment of the ALS and TLS data is required. However, instead of registering all N TLS scans directly to the ALS data, we choose to separately align the ALS data to each of the N TLS point clouds or scan locations. This condition allows us to preserve the shape of the crowns measured by the TLS system, and to adapt the ALS segmentation result to the fine resolution crown profile, measured via the TLS data. Note that the proposed method does not superimpose the crowns polygons delineated in the ALS data onto the TLS data, but rather fits the segmentation result to the terrestrial data due to the Euclidean transformation applied to the ALS segmented image to fit the TLS scan.

Because of the different acquisition perspectives, the terrestrial point clouds ($P_{t,1} \dots P_{t,n} \dots . P_{t,N}$) and the airborne point cloud (P_a) sample different surfaces of the forest structure, and thus cannot be automatically registered (see Fig. 2) [53]. This has been addressed in several ways in the literature [36]. Here, we present a novel approach, by taking advantage of the fact that for certain forest conditions, e.g., open woodland savanna, the measured forest structure (i.e., spatial distribution of the trees) is similar in both the airborne and terrestrial LiDAR data. We acknowledge that this is not always the case, especially for closed canopies where a terrestrial instrument is unable to reach the upper canopy. However, the proposed method can be adapted to the closed canopy case by considering further structural features, since the two data types still represent the same forest structure (i.e., the stems measured by the TLS data correspond to the tree tops visible in the ALS).

For open woodland study areas, e.g., the study area in our case, it is possible to take advantage of the correlation between the 2-D height profiles of the horizontal forest structure (i.e., the CHM's I_a and $I_{t,1} \dots I_{t,n} \dots . I_{t,N}$), as measured by the ALS and the TLS instruments, in order to determine appropriate registration parameters. In other words, we leverage the consistent representation of the spatial distribution of canopies in order to align ALS data to the TLS scans via correlation-based image registration between the appropriate CHMs.

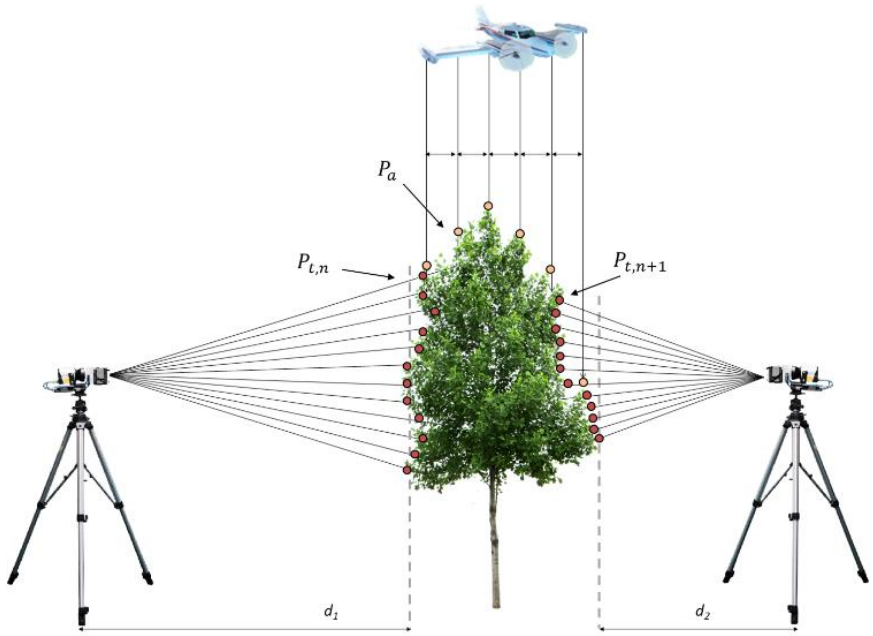

Fig. 2. Visual representation of the different surfaces sampled for the same tree scanned by ALS and multiangular TLS. Due to the different measurement perspectives, the LiDAR point cloud data are not directly comparable.

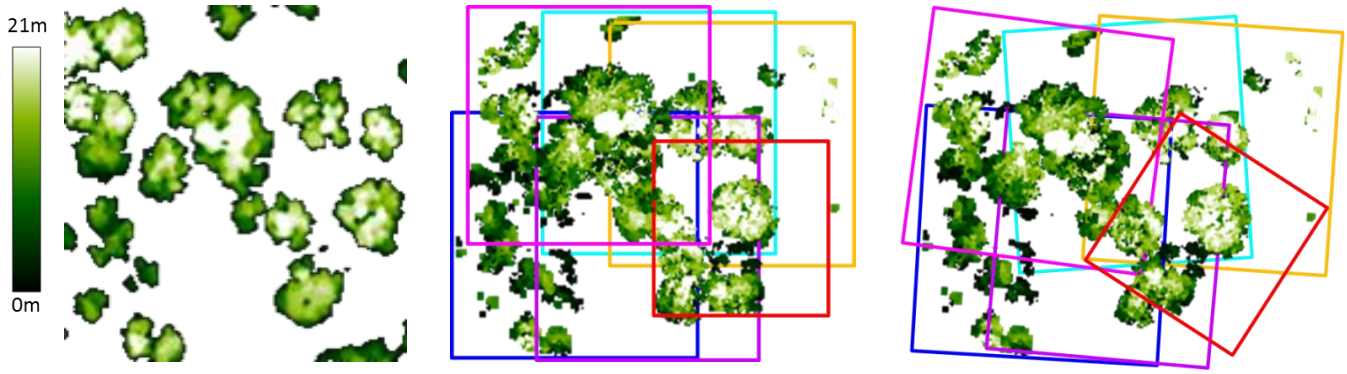

Fig. 3. Example of the registration of the TLS scans to the ALS coordinate system. For the same forest area, a false color representation of the CHM is shown for (a) ALS data, (b) original TLS scans merged, and (c) registered TLS scans merged. For each TLS scan, the best Euclidean transformation is calculated in order to match the horizontal structure of the forest represented in the ALS data.

Let us consider the n^{th} scan $I_{t,n}$ and let $M \times L$ be the pixels size of $I_{t,n}$. In the first step, parameters of a planar Euclidean transformation, $E_{a,n}$, are estimated in order to register the ALS CHM, I_a, to the TLS CHM, $I_{t,n}$. Initial estimates for the three degrees of freedom of $E_{a,n}$ were obtained from coarse *in situ* GPS measurements at each scan location and nominal orientation during data collection. In other words, the CHM of the airborne data, I_a, is first centered to the GPS coordinates of the TLS scan, $I_{t,n}$ (i.e., so that initial translation estimates are zero), and cropped to keep the approximate portion of the airborne CHM, I_a, thus representing the same forest area present in $I_{t,n}$. Parameter optimization of a planar Euclidean transformation matrix, $E_{a,n}$ [see (1)], is then performed in the context of a gradient descent optimization framework [54], [43]. The planar Euclidean transform applied to $I_{a,n}$ maps the image from its original coordinate system to the coordinate system of the reference image $I_{t,n}$, that is

$$E_{a,n}(x,y) = \begin{pmatrix} cos\phi & -sin\phi \\ sin\phi & cos\phi \end{pmatrix} \begin{pmatrix} x \\ y \end{pmatrix} + \begin{pmatrix} t_x \\ t_y \end{pmatrix} \quad (1)$$

where ϕ is the rotation angle and $[t_x, t_y]$ the translation vector. Gradient descent optimization seeks to estimate the three unknown parameters by minimizing the sum of squared differences (SSD) between the terrestrial CHM, $I_{t,n}$, and the registered airborne, CHM $I'_{a,n}$, as follows:

$$SSD_{min} = \min_{\phi,t_x,t_y} \sum_{i=1}^{M} \sum_{j=1}^{L} \left[I_{t,n}(x_i, y_j) - I_{a,n}\left(E_{a,n}(x_i, y_j)\right) \right]^2 = \min_{\phi,t_x,t_y} \sum_{i=1}^{M} \sum_{j=1}^{L} \left[I_{t,n}(x_i, y_j) - I'_{a,n}(u_i, v_j) \right]^2 \quad (2)$$

where $u_i = (x_i \cdot cos\phi - y_j \cdot sin\phi) + t_x$ and $v_j = (x_i \cdot sin\phi + y_j \cdot cos\phi) + t_y$. For each nth terrestrial scan we can

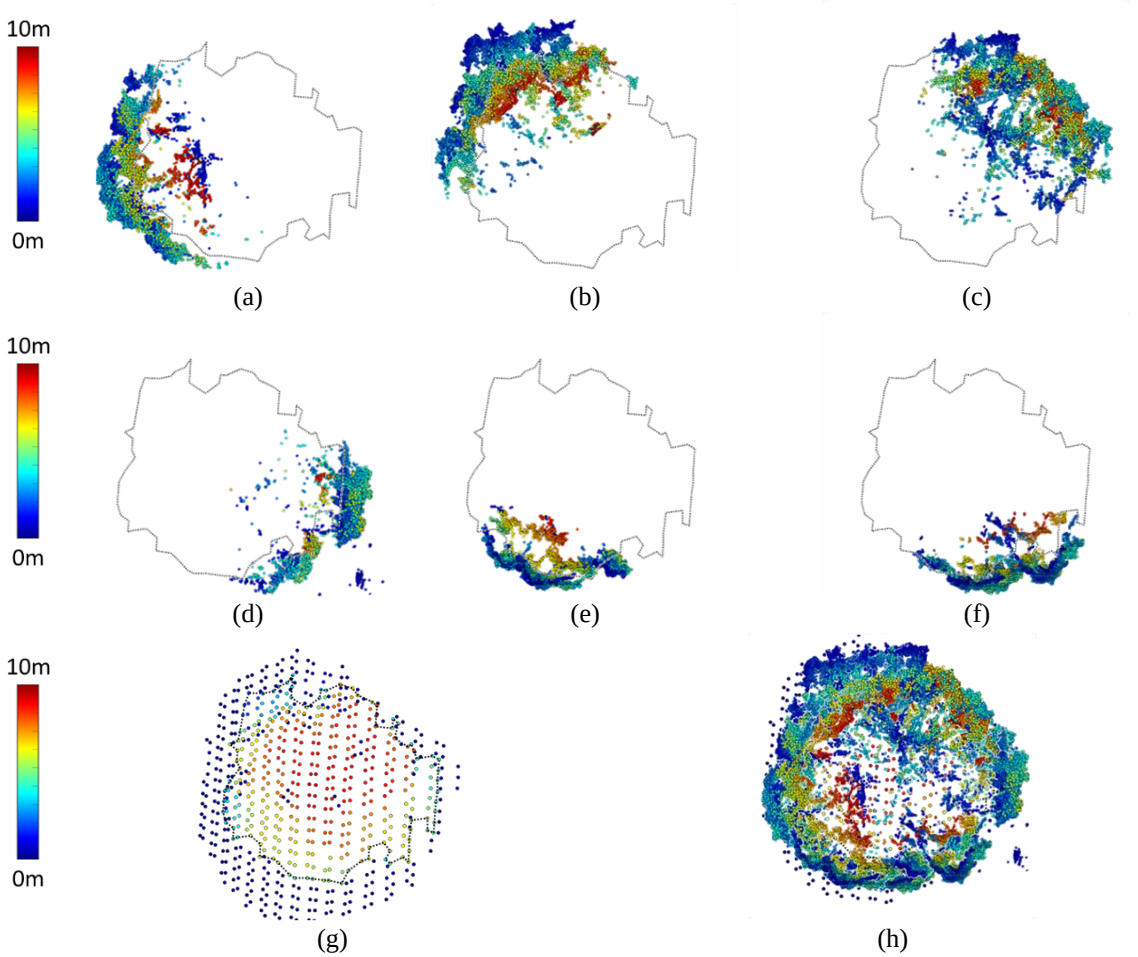

Fig. 4. Example of the 3-D point cloud fusion step. For the same crown, a top view is shown for (a)-(f) TLS data, (g) ALS data, and (h) fused data.

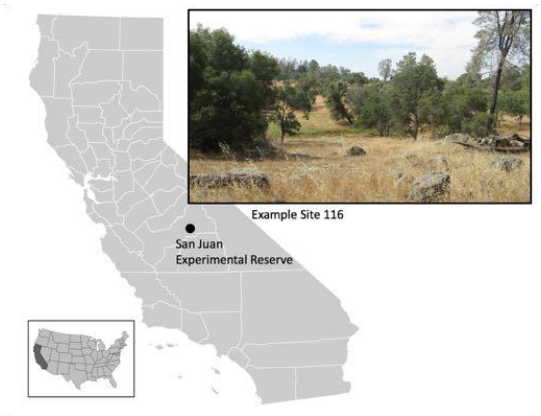

Fig. 5. NEON PWS D17 is located in Central California. It contains one core site and two relocatable sites. The core site, the SJER, is an oak savanna.

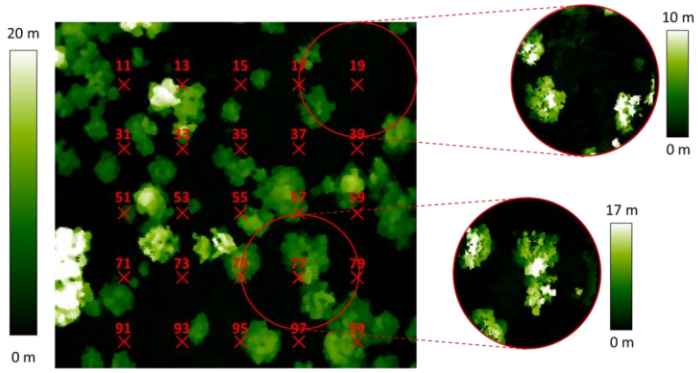

Fig. 6. (Left) False color representation of the ALS CHM. The approximate TLS measurement locations are marked in red along with the acquisition number. (Right inset) CHMs obtained for two examples of TLS scans are provided.

calculate the planar Euclidean transformation, $E_{a,n}$, which allows us to register $I_{a,n}$ to each $I_{t,n}$. Therefore, TLS segmentation is performed by applying the ALS-derived segmentation result onto each TLS scan, after first registering the ALS data, I_a, to the coordinate space of each TLS data, $I_{t,1} \ldots I_{t,n} \ldots . I_{t,N}$, using the obtained transformation parameters. This condition enables us to adapt the segmentation performed on the ALS data to the TLS scans, thereby preserving the fine-resolution profile of the crown shape. The result is a set of canopy segmentation maps for the TLS data, $S_{t,1} \ldots S_{t,n} \ldots . S_{t,N}$, which correspond to that obtained from the ALS data

C. *Three-Dimensional Point Cloud Fusion*

The final phase, *fusion*, seeks to fuse the segmented crowns in the 3-D point cloud space. First, we need to align the ALS point cloud and the N TLS point clouds into a common coordinate system, i.e., those of the ALS data. Note

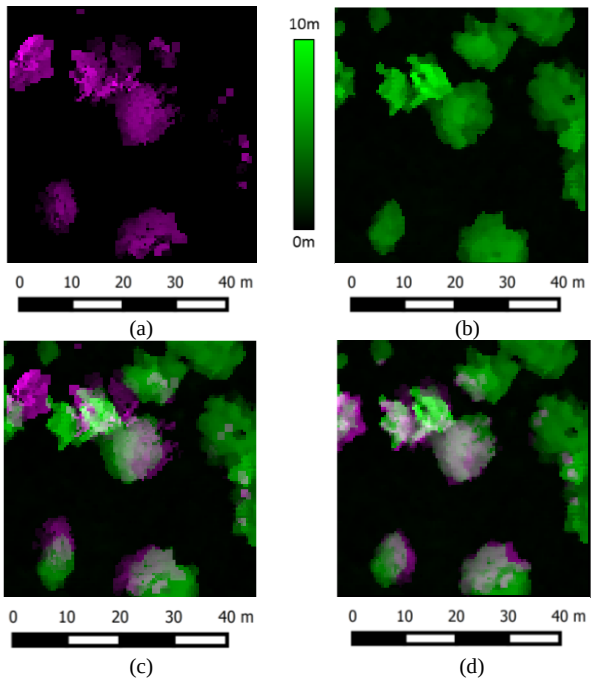

Fig. 7. Qualitative example of TLS scan registration results. (a) False color representation of the original TLS CHM (pink patches) for the 75th scan of Site 116. (b) False color representation of the ALS CHM (green patches) for the 75th scan of Site 116. (c) Original TLS CHM (pink patches) is overlapped with the ALS CHM (green patches). (d) Registered TLS CHM (pink patches) is overlapped with the ALS CHM (green patches). Although the registration is accurately performed, the obtained correlation similarity measure Ψ is 0.62 because of the missed detection of some trees by the TLS due to tree occlusions.

that the comprehensive representation of the horizontal structure of the forest provided by the ALS data allows us to automatically register the TLS scans without the need for positioning reference targets on the ground during the data acquisition campaign (see Fig. 3).

Similar to the previous case, we aim to estimate the planar Euclidean transformation that allows the registration of each TLS CHM, $I_{t,n}$, to the ALS CHM, I_a. Thus, the considered transformation is the inverse of the previous transformation (1). Accordingly, the planar Euclidean transformation, $E_{t,n}$, applied to $I_{t,n}$ to match I_a is defined as follows:

$$E_{t,n}(x,y) = \begin{pmatrix} cos\theta & -sin\theta \\ sin\theta & cos\theta \end{pmatrix} \begin{pmatrix} x \\ y \end{pmatrix} + \begin{pmatrix} h_x \\ h_y \end{pmatrix} \quad (2)$$

where $\theta = -\phi$, $h_x = -t_x$, and $h_y = -t_y$. To evaluate the effectiveness of the registration process, we compute the normalized cross correlation similarity measure between $I_{a,n}$ and $I'_{t,n}$. The value of the correlation image I_{corr} at the position (w, l) is computed as follows:

$$I_{corr}(w,l) = \frac{\sum_{x,y}[I_{a,n}(x,y) - \mu_{a,n}][I'_{t,n}(x-w, y-l) - \mu_{t,n}]}{\sqrt{\sum_{x,y}[I_{a,n}(x,y) - \mu_{a,n}]^2 \sum_{x,y}[I'_{t,n}(x-w, y-l) - \mu_{t,n}]^2}} \quad (3)$$

where $\mu_{a,n}$ and $\mu_{t,n}$ are the mean values, i.e., height, of $I_{a,n}$ and $I'_{t,n}$, respectively. Automatic validation of the registration result is achieved by checking the resulting normalized correlation matrix, I_{corr}, obtained at the end of the registration step. In other words, we can confirm if the position of the peak (X_p, Y_p) is the center of the correlation matrix (i.e., [0 0]) and the value of the peak $\Psi \in [-1, 1]$ is higher than a positive threshold. The segmentation results obtained in the image domain, i.e., $S_{t,1} \ldots S_{t,n} \ldots . S_{t,N}$ and S_a, then are transferred to the 3-D point cloud space.

For each delineated 3-D crown belonging to the *n*th TLS scan, we apply the obtained transformation, thus registering the data to the airborne coordinate system. At the end of the registration phase, the proposed method performs the fusion of the ALS and TLS point clouds per crown (according to the registered ALS and TLS segmented maps) to generate the set of final fused 3-D segmented point clouds. Fig. 4 shows a qualitative example of the result obtained by fusing the 3-D ALS and TLS segmented point clouds.

III. Data Set Description

The study area for the project is the National Ecological Observatory Network (NEON) Pacific Southwest (PWS) Domain 17 (D17) core site, located in the San Joaquin Experimental Range (SJER; 37°6'43,77'' N, 119 44°11',85"), near Fresno, CA, USA. The SJER is oak savanna woodland (see Fig. 5). The dominant species are blue oak (*Quercus Douglasii*), interior live oak (*Quercus Wislizeni*), and grey pine (*Pinus Sabiniana*). Ground reference data were collected in June 2013 for 27 trees in the considered study area. The height, species, diameter at breast height (DBH), and crown width of each tree were measured at each sample location.

ALS data were obtained from the NEON airborne observation platform (AOP), which operates an Optech Airborne Laser Terrain Mapper (ALTM) Gemini LiDAR system. The 1064nm, four-return-per-pulse system was operated at a 100 kHz pulse repetition rate at 1000 m above-ground-level (AGL), for an average point density of 2 hits/m^2. The ALS overflight was executed coincident with the TLS field measurement campaign, during the period of June 9-21, 2013.

We used a second-generation, low-cost terrestrial LiDAR system, integrated from commercial-off-the-shelf components by Rochester Institute of Technology in collaboration with University of Massachusetts Boston [55]. This TLS is dubbed the canopy biomass LiDAR, and is based on a design first implemented by a team at the Katholieke Universiteit Leuven, Belgium [56]. Unlike many commercial scanners that provide for high-density point cloud data, lower-cost systems are geared toward efficient and fast sampling of structural data, often at a much lower resolution or point spacing. This system has a minimum angular step width of 4.36 mrad, and a beam divergence of 15 mrad, both approximately two orders of magnitude coarser than comparable commercial instrumentation [55].

The sensor head consists of a SICK LMS-151 laser scanner, which is compact, lightweight (1.1 kg), and weather-resistant (SICK, 2009). A 905 nm laser is pulsed at 27 kHz with range measurement recorded based on time of flight; up to two returns per outgoing pulse are digitized. The laser pulse is deflected by a rotating mirror to sample a 270° arc, swept out in elevation angle. This sensor head is coupled to an azimuthal rotation stage, which provides coverage of the full hemisphere above the instrument and a portion of the hemisphere below, i.e., 270° in

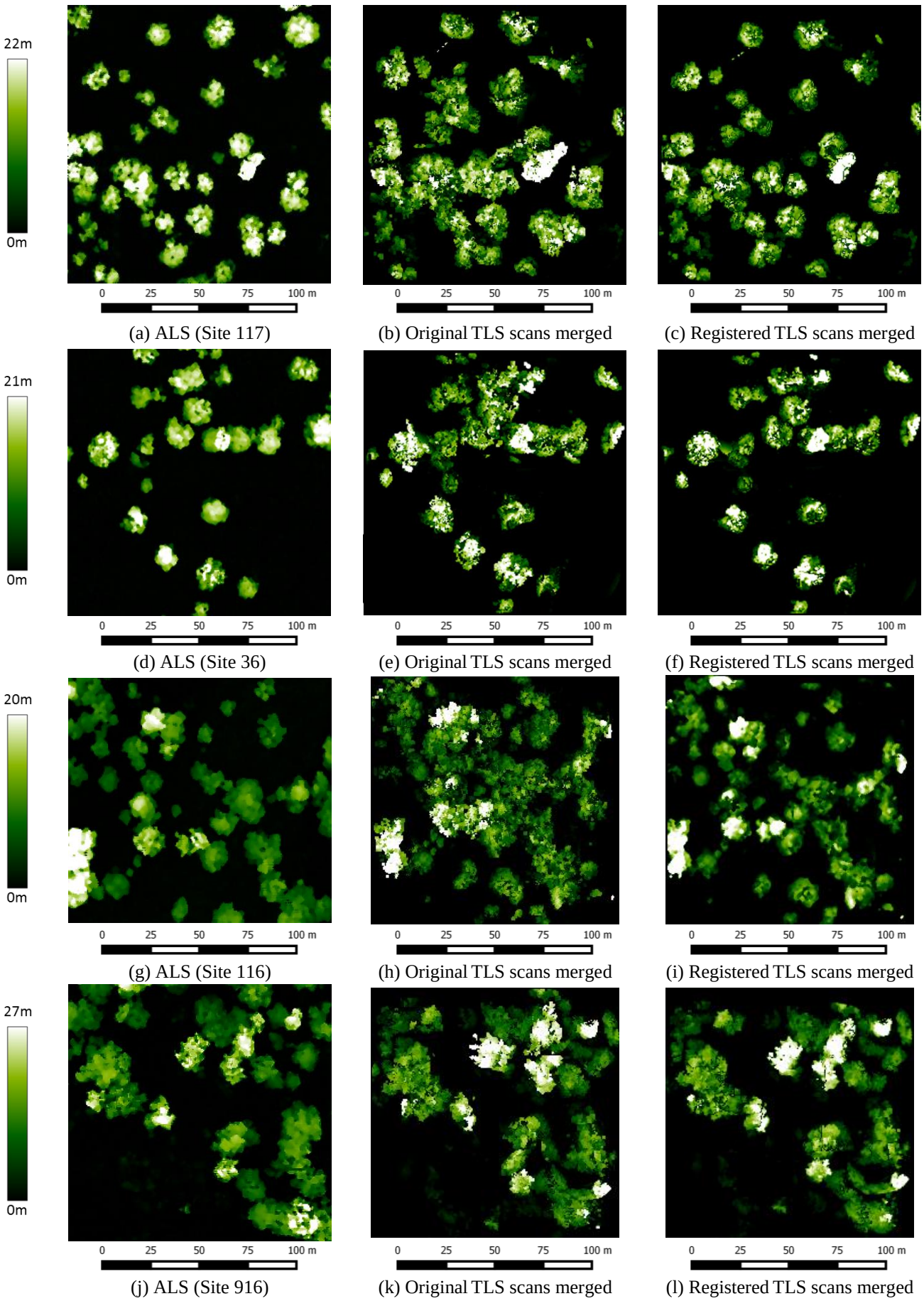

Fig. 8. Final registration results. (Left column) ALS data. (Middle column) Original TLS data merged. (Right column) Registered TLS data merged.

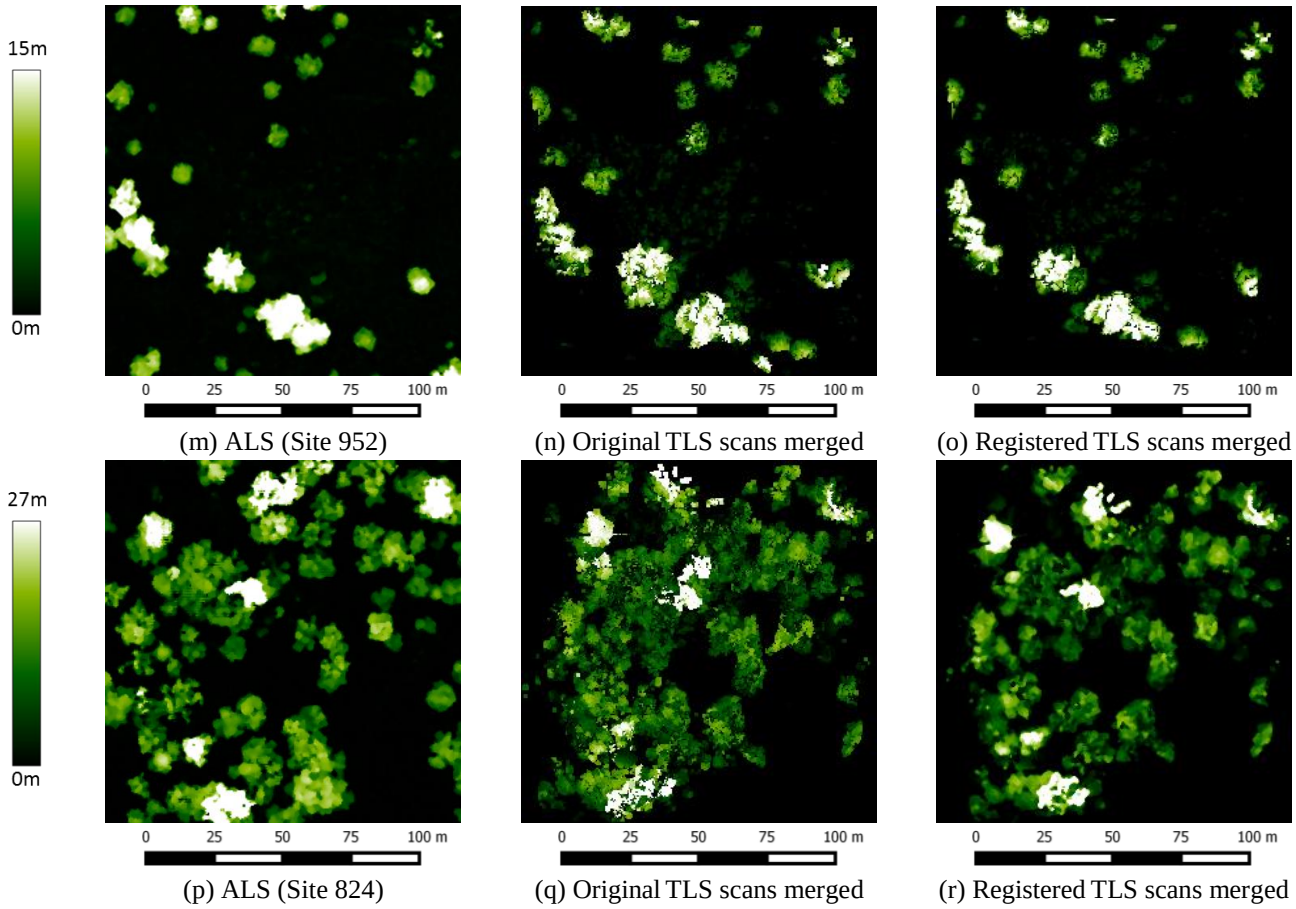

Fig. 8. (*Continued*) Final registration results. (Left column) ALS data. (Middle column) Original TLS data merged. (Right column) Registered TLS data merged.

the zenith (vertical) and 360° in the azimuth (horizontal) planes. A BeagleBone computer and power tool battery are mounted to the unit, while sensor control is achieved via a wireless mobile application.

Six plots of 40 m × 40 m, 25 scans per plot, were collected along an equally spaced grid at 10 m increments (see Fig. 6). Among the 150 terrestrial scans collected, 19 of them were discarded due to acquisition problems, such as no-data scans. No artificial targets were placed in plots to aid the terrestrial data acquisition and registration. The plots were laid out by means of the traditional tape-and-compass method, following a GPS measurement of plot center. This regular sampling acquisition setup allowed us to acquire fast but consistent data coverage.

IV. Experimental Results and Discussion

In this section, first we analyzed the global registration results obtained when we align the N TLS scans to the ALS data. This was done by reprojecting the TLS scans into the ALS coordinate system (Section II-C). Then, we evaluate the crown parameter estimation performed on the obtained set of 3-D fused crowns. Both these analyses are presented from a qualitative and a quantitative perspective.

A. Registration Results

Fig. 8 shows the ALS data and the composition of the TLS scans, before and after the registration, for each site of the considered data set. Fig. 8 graphically demonstrates the importance of performing the registration phase, since the original TLS scans are shifted with respect to the ALS data because of the inaccurate GPS position estimation and the different acquisition perspectives. This misalignment is clearly visible when merging the original TLS data with respect to the registered TLS scans. In contrast, the horizontal structure of the forest, represented by the fusion of the registered TLS scans, is coherent with the structure represented in the ALS data using the proposed technique.

For quantitative evaluation, we compared the normalized cross correlation between ALS data and TLS scans before and after the global registration procedure. In particular, the evaluation was performed by considering both the value Ψ and the peak position (X_p, Y_p) of the resulting normalized correlation image. Table I reports the minimum, median, and maximum values of Ψ and (X_p, Y_p) summarized per site, while in Tables II and III, the correlation similarity metrics are presented per terrestrial scan. The proposed method always improves the correlation coefficient values with respect to the initial registration given by the coarse GPS measurements of the TLS scans center (Table I). The obtained similarity peak, Ψ, is characterized by an overall median value of 0.73, in contrast to the 0.65 median value of the initial registration result. However, for some scans the value of the correlation peak is lower than 0.55, even though the Euclidean transformation accurately registers the ALS and the TLS data. These results are due to the different acquisition perspectives that lead to the presence of specific differences in the ALS and TLS CHMs

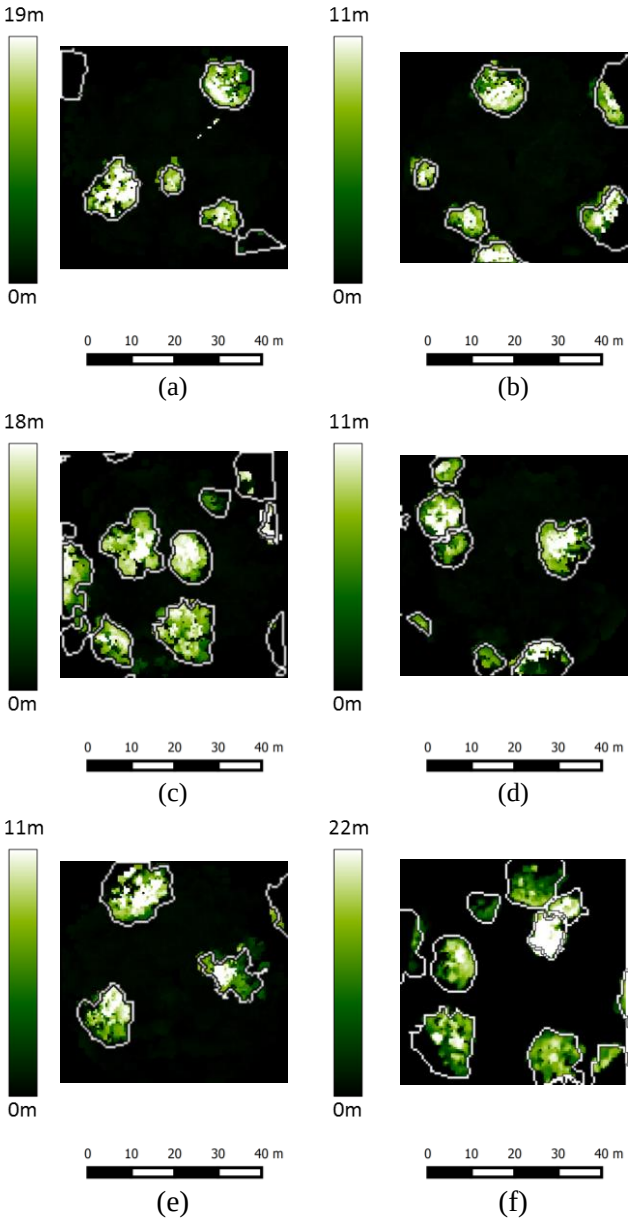

Fig. 9. (a)-(f) Qualitative example of TLS scan registration results. The final boundaries of the TLS segmented crowns are highlighted in white and overlapped with the false color representation of the TLS CHMs.

acquired over the same forest stand. While the ALS accurately represents the horizontal structure of the forest from a top-down perspective, the TLS may miss some trees present in the scene due to occlusion, caused by trees that surround the scanner [57]. However, the surrounding trees are sufficient to describe a specific forest structure that can be easily identified in the ALS data, i.e., the omitted trees, located in the background of the TLS scans, are not critical to algorithm performance. Fig. 7(a) and (b) represents the TLS CHM and the ALS CHM of the 75th scan of the 116th site, respectively. Although the registration is accurately performed [see Fig. 7(d)], the obtained correlation similarity measure, Ψ, is 0.57 because of the omission of some trees by the TLS due to tree occlusions.

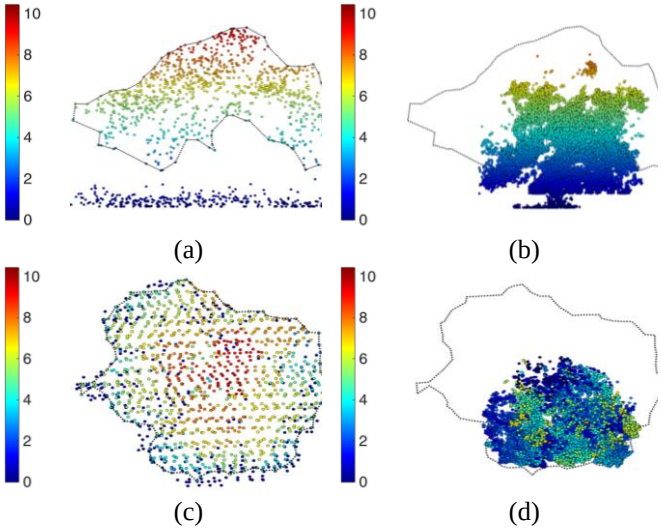

Fig. 10. Qualitative example of the complementary information provided by ALS and one single TLS scan. (a) Side view of the ALS data, (b) side view of the TLS data, (c) top view of the ALS data, and (d) top view of the TLS data for the same tree crown. While the airborne acquisition accurately represents the horizontal structure of the crown, the terrestrial scanner provides a very high resolution profile of the bottom part of the canopy.

However, the location of the correlation peak is [0,0]. Note that for all the TLS scans, the correlation peak location obtained is almost [0,0], regardless of the stand forest structure measured (see Table III). This is different from the initial registration results (see Table II), which exhibit significant biases. It also is possible to verify that the resulting metrics are better than those obtained without performing any registration (i.e., from the original LiDAR data), over and above an assessment of the value of the correlation peak and its location.

Moreover, it is important to consider that the proposed method is automatic and does not require any parameter tuning to perform the registration, since it is completely driven by the spatial distribution of the trees present in the scene. Furthermore, even though in the considered ALS data set we are employing low-density airborne LiDAR data (2 pts/m^2), the use of the rasterized version of the LiDAR point cloud to perform the registration overcomes the limitations introduced by the relatively low laser sampling density. It thus follows that no strict laser density requirements are needed in terms of the acquisition of ALS data.

B. Crown Parameter Estimation Results

The final phase of the proposed method performs the fusion of the segmented ALS and TLS LiDAR point clouds in the 3-D point cloud space. Fig. 9 shows a qualitative example of the TLS crown segmentation result, obtained by registering the ALS crown boundaries to the TLS data. Due to the registration of the segmented ALS image to the TLS data, the crown boundaries delineated in the LAS data are adapted to the shape of the crown measured by the terrestrial laser scanner.

It is worth noting that the registration phase is not affected by the airborne segmentation result, which is performed on the original CHMs. In contrast, the accuracy of the TLS segmentation strongly depends on the ALS crown delineation

TABLE I

MAXIMUM, MINIMUM AND MEDIAN VALUES OF THE PEAK Ψ AND THE POSITION OF THE PEAK (X_p, Y_p) OF THE RESULTING NORMALIZED CROSS CORRELATION SIMILARITY VALUES PER SITE OBTAINED BEFORE AND AFTER THE REGISTRATION STEP.

		Not registered			Registered		
		Min	**Median**	**Max**	**Min**	**Median**	**Max**
Site 116	Ψ	0.37	0.57	0.75	0.57	0.71	0.84
	X_p	0	3	72	0	0	0
	Y_p	0	3	50	0	0	0
Site 117	Ψ	0.31	0.62	0.79	0.54	0.73	0.84
	X_p	0	4	55	0	0	1
	Y_p	1	4	61	0	0	2
Site 916	Ψ	0.42	0.64	0.85	0.51	0.69	0.87
	X_p	0	5	31	0	0	1
	Y_p	0	4	12	0	0	1
Site 952	Ψ	0.42	0.69	0.86	0.59	0.77	0.87
	X_p	0	2	9	0	0	1
	Y_p	0	4	9	0	0	1
Site 36	Ψ	0.34	0.72	0.88	0.59	0.76	0.89
	X_p	0	3	8	0	0	1
	Y_p	0	4	11	0	0	2
Site 824	Ψ	0.31	0.60	0.77	0.53	0.66	0.80
	X_p	0	4	20	0	0	1
	Y_p	0	4	70	0	0	1
All	Ψ	0.31	0.65	0.88	0.53	0.73	0.89
	X_p	0	3	72	0	0	1
	Y_p	0	4	70	0	0	2

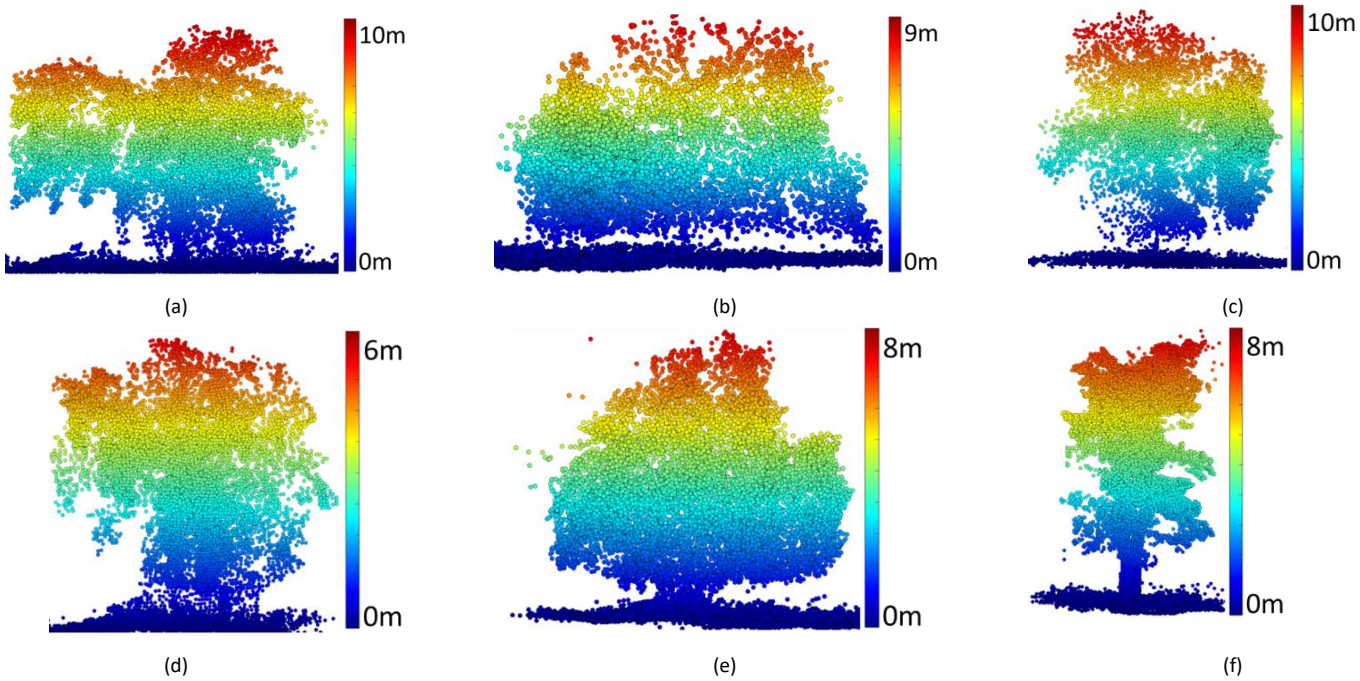

Fig. 11. (a)–(f) Qualitative examples of obtained fused crowns.

result. The ALS segmentation, due to the top view perspective, achieves higher segmentation accuracy when compared to the TLS, even though the terrestrial data provide a higher (finer) resolution point cloud. Moreover, based on the ALS segmentation result, the proposed method allows us to automatically extract the TLS crowns without performing any further analysis or refinement.

Fig. 10 shows a comparison between the ALS data and one of the singular TLS scans, acquired for one of the trees of the considered data set. The presented results confirm the complementarity of ALS and TLS LiDAR data. The airborne data provide a comprehensive representation of the horizontal structure of the forest and of the entire uppermost part of the canopies, which allow us to drive the registration of the TLS scans in an automatic fashion and to perform crown delineation.

However, due to the low laser sampling density and the top view acquisition perspective, ALS data alone do not adequately describe the below-canopy structure. TLS, on the other hand,

TABLE II
NORMALIZED CROSS CORRELATION SIMILARITY VALUES OF THE ORIGINAL LIDAR DATA (NOT REGISTERED). FOR EACH TERRESTRIAL SCAN THE OBTAINED CORRELATION COEFFICIENT $\Psi \in [-1,1]$ AND THE POSITION (X_p, Y_p) OF THE CORRELATION PEAK ARE GIVEN. THE DESIRED POSITION OF THE CORRELATION PEAK IS [0,0], WHICH CORRESPONDS TO THE CENTER OF THE CORRELATION MATRIX.

	Site116			**Site117**			**Site916**			**Site952**			**Site36**			**Site824**		
	Ψ	X_p	Y_p	Ψ	X_p	Y_p	Ψ	X_p	Y_p	Ψ	X_p	Y_p	Ψ	X_p	Y_p	Ψ	X_p	Y_p
11	0.71	-6	6	0.56	-3	5	0.58	-3	4	0.64	5	0	0.70	3	1	0.60	-13	6
13	0.54	3	1	0.69	-4	7	0.51	4	1	0.71	2	-1	0.34	6	4	0.33	15	18
15	-	-	-	0.69	0	11	0.75	4	2	0.66	1	-2	0.40	8	2	0.48	4	-70
17	0.61	2	-3	0.65	-3	2	-	-	-	0.68	1	-4	0.58	-4	4	0.31	-20	-31
19	0.59	9	0	-	-	-	0.75	0	-1	0.71	3	-4	0.47	3	2	0.65	6	4
31	0.39	-1	49	0.68	0	15	0.42	-5	-1	0.52	-5	-2	0.71	0	3	-	-	-
33	0.56	-24	4	0.69	4	5	0.69	0	1	0.70	-1	1	0.57	5	-2	0.72	-6	-2
35	0.72	-8	3	0.36	55	4	0.73	-7	5	0.66	-2	-4	0.64	2	1	0.60	-5	4
37	0.55	-7	11	0.51	-47	-61	0.71	-8	0	-	-	-	-	-	-	0.32	0	-53
39	0.42	-72	50	0.59	6	3	0.54	5	-3	-	-	-	0.77	-1	-1	0.45	-5	0
51	-	-	-	0.31	-4	1	-	-	-	0.77	-1	-4	0.72	3	4	0.54	-4	9
53	0.67	-2	8	0.65	-8	2	0.55	0	6	0.77	-2	-5	0.70	2	-1	0.64	3	6
55	0.71	3	-2	0.75	-4	6	0.85	0	3	0.73	-2	1	0.74	6	-7	0.73	0	3
57	0.49	5	-2	0.62	-1	7	0.83	5	7	-	-	-	0.73	0	-4	0.77	0	0
59	0.55	8	-1	0.79	0	4	0.73	2	-6	-	-	-	0.80	2	6	0.67	0	-3
71	0.72	-9	-5	0.59	-7	6	0.53	-3	-8	0.75	-2	3	0.81	1	8	0.36	-4	8
73	0.58	-3	-5	0.62	2	4	-	-	-	0.86	-9	6	0.82	1	5	0.60	-2	-4
75	0.41	2	1	0.68	7	1	-	-	-	0.53	-2	-5	0.60	4	8	0.47	-4	-4
77	0.52	3	3	0.53	13	1	0.52	31	12	0.44	-8	-4	0.66	-1	0	0.61	1	-1
79	0.67	3	6	0.69	4	1	0.50	3	-4	0.79	-3	7	-	-	-	0.65	1	-1
91	-	-	-	0.64	1	2	0.69	-5	2	0.65	1	0	0.73	1	11	0.50	-14	-36
93	-	-	-	0.55	0	-1	0.56	-8	-4	0.60	0	-7	0.88	3	7	0.68	0	8
95	0.58	0	0	0.44	3	5	0.56	-5	-12	0.78	0	-9	0.80	3	3	-	-	-
97	0.75	0	-6	0.53	6	4	0.75	-4	0	0.84	-3	0	0.72	5	0	-	-	-
99	0.37	12	2	0.68	0	4	0.59	11	9	0.42	7	6	0.77	4	4	-	-	-

provides a high resolution profile of the bottom portion of the tree crowns. A more comprehensive representation of the crown structure therefore is available via the fusion of information from both the TLS and ALS data sets or perspectives.

Fig. 11 shows select examples of 3-D fused point clouds, while Fig. 12 depicts the number of points per tree. These results point out that the proposed fusion method automatically leads to very high density LiDAR point clouds per crown.

Note that the resolution (or point density) of the obtained crowns varies, depending on: 1) the number of associated TLS scans; 2) the distance of the laser from the crown during the acquisition; and 3) the topography of the scene, since the TLS acquisitions are not performed in homogeneous conditions for all the scans, e.g., on steep slopes, occlusion problems could arise.

The considered TLS measurement setup was designed in order to have a fast and practical acquisition campaign and to obtain a regular sampling of the study area. However, to increase the point density and associated resolution for the fused tree crowns, the number of TLS acquisitions can be increased, multiple TLS scans can be acquired around each tree, and the ALS point density can be increased via adapting specific flight parameters, e.g., flight overlap, scan frequency, and pulse frequency.

Fig. 13 and Table IV present the quantitative analysis of the crown parameter estimation, obtained from the set of fused crowns. For each tree, the height of the tree, the crown width, and the 90° crown width were compared with the ground reference data. The crown volume, calculated by using the alpha shape on the obtained fused data, furthermore was correlated with the measured DBH. We determine the two crown widths by considering the length of the major and the minor axis of the ellipse having the same normalized second central moments of the crown region, since the tree top height itself is associated with the highest LiDAR point belonging to that crown.

We concluded from these results that the fusion accurately estimated the crown parameters by taking advantage of the

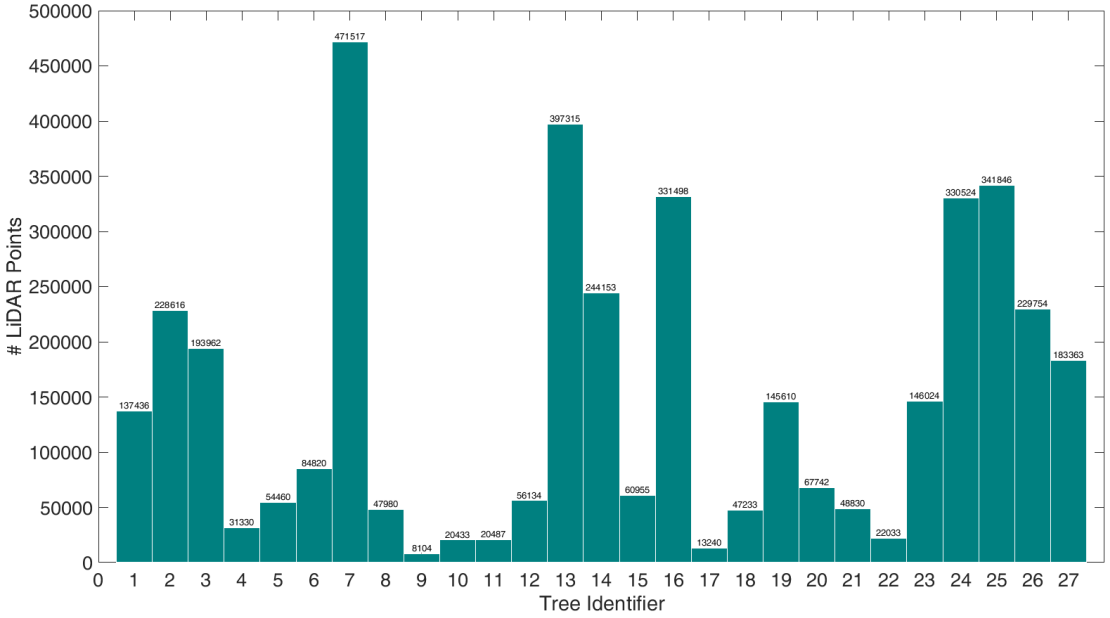

Fig. 12. Number of LiDAR points per fused crown.

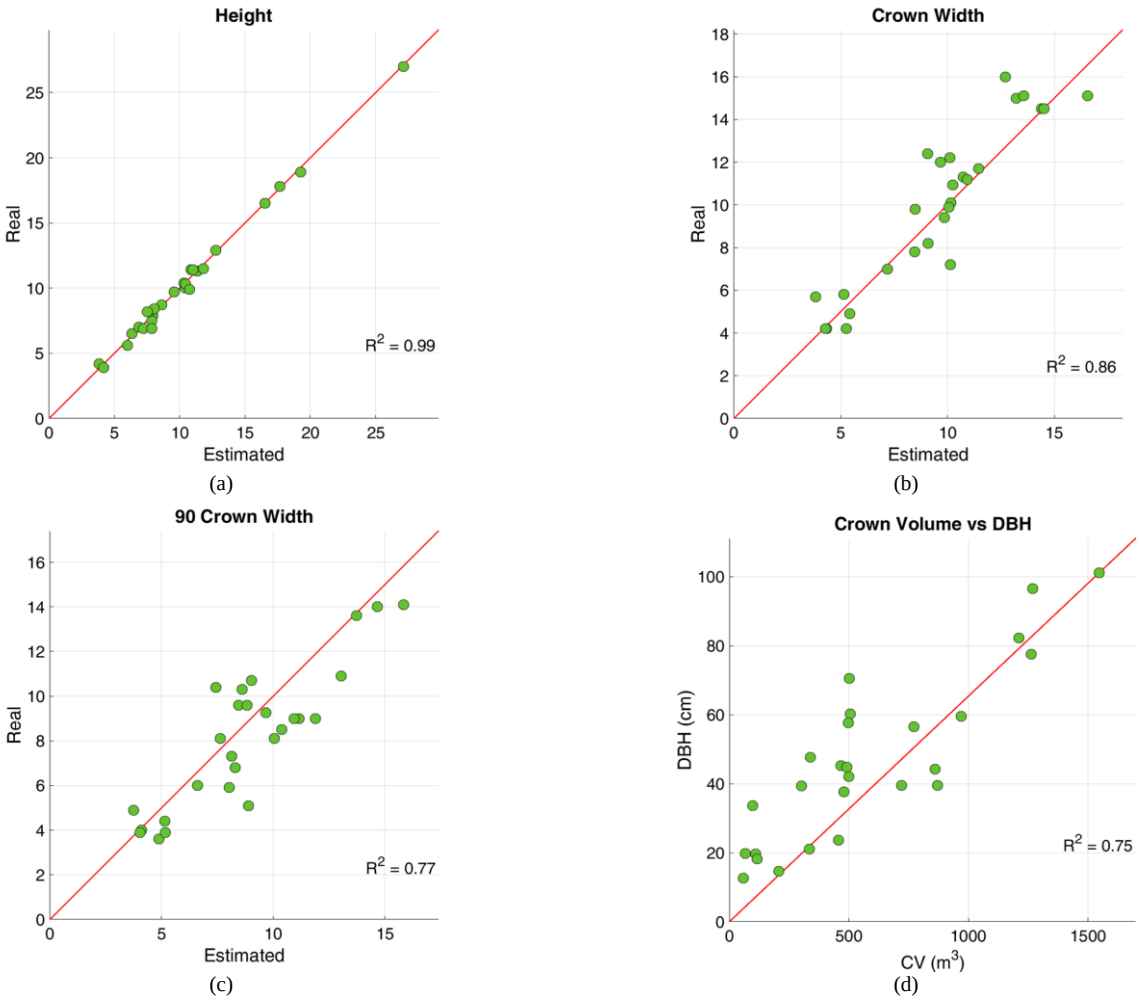

Fig. 13. Crown parameter estimation results obtained on the set of fused ALS and TLS data sets. (a) Tree top height. (b) Crown width. (c) 90° crown width. (d) Correlation between the estimated crown volume and the measured DBH.

combination of the complementary acquisition viewpoints, i.e. ALS vs. TLS. The proposed method obtained an average coefficient of determination (R^2) of 0.98 on the tree-top height, 0.86 on the crown width, and 0.77 on the 90° crown width by combining the two information sources. Moreover, the high resolution 3-D point clouds obtained enable an accurate

.TABLE III
NORMALIZED CROSS CORRELATION SIMILARITY VALUES OBTAINED AFTER THE REGISTRATION STEP. FOR EACH TERRESTRIAL SCAN THE OBTAINED CORRELATION COEFFICIENT $\Psi \in [-1,1]$ AND THE POSITION (X_p, Y_p) OF THE CORRELATION PEAK ARE GIVEN. THE DESIRED POSITION OF THE CORRELATION PEAK IS [0,0], WHICH CORRESPONDS TO THE CENTER OF THE CORRELATION MATRIX.

	Site116			**Site117**			**Site916**			**Site952**			**Site36**			**Site824**		
	Ψ	X_p	Y_p	Ψ	X_p	Y_p	Ψ	X_p	Y_p	Ψ	X_p	Y_p	Ψ	X_p	Y_p	Ψ	X_p	Y_p
11	0.75	0	0	0.82	0	0	0.58	0	1	0.81	0	0	0.72	0	-1	0.66	0	0
13	0.84	0	0	0.78	0	0	0.67	-1	0	0.76	0	0	0.59	0	0	0.68	0	0
15	-	-	-	0.74	0	0	0.83	0	0	0.72	0	1	0.62	0	0	0.64	0	0
17	0.77	0	0	0.80	0	0	-	-	-	0.77	0	1	0.73	0	0	0.53	0	0
19	0.78	0	0	-	-	-	0.79	0	0	0.78	0	0	0.62	0	0	0.65	0	0
31	0.69	0	0	0.73	0	0	0.67	0	0	0.62	1	0	0.79	0	0	-	-	-
33	0.71	0	0	0.73	0	0	0.70	0	0	0.78	0	0	0.65	0	0	0.75	0	0
35	0.76	0	0	0.76	0	0	0.64	-1	0	0.76	0	1	0.67	0	0	0.60	1	0
37	0.68	0	0	0.66	1	-2	0.74	0	1	-	-	-	-	-	-	0.72	0	0
39	0.59	0	0	0.75	0	0	0.55	0	0	-	-	-	0.80	0	0	0.70	0	0
51	-	-	-	0.54	0	0	-	-	-	0.84	0	0	0.80	0	0	0.54	0	0
53	0.72	0	0	0.73	0	0	0.65	0	0	0.82	0	0	0.82	0	0	0.67	0	0
55	0.73	0	0	0.75	0	0	0.87	0	0	0.75	0	0	0.81	0	0	0.75	0	0
57	0.62	0	0	0.71	0	0	0.81	0	-1	-	-	-	0.82	0	0	0.80	0	0
59	0.60	0	0	0.82	0	0	0.75	-1	-1	-	-	-	0.72	1	-2	0.79	0	0
71	0.81	0	0	0.66	0	0	0.61	0	0	0.82	0	0	0.79	0	0	0.57	0	0
73	0.79	0	0	0.68	0	0	-	-	-	0.87	0	0	0.88	0	0	0.62	0	0
75	0.57	0	0	0.71	0	0	-	-	-	0.59	1	0	0.72	0	0	0.60	0	0
77	0.60	0	0	0.70	0	0	0.76	0	1	0.62	0	0	0.70	0	0	0.64	1	-1
79	0.65	0	0	0.78	0	0	0.54	-1	1	0.80	0	0	-	-	-	0.73	0	0
91	-	-	-	0.67	0	0	0.75	0	0	0.68	0	0	0.80	0	0	0.65	0	0
93	-	-	-	0.58	0	0	0.68	0	0	0.74	0	0	0.89	0	0	0.73	0	0
95	0.72	0	0	0.84	0	0	0.63	1	1	0.80	0	0	0.84	0	0	-	-	-
97	0.79	0	0	0.68	0	0	0.76	0	0	0.87	0	0	0.70	0	0	-	-	-
99	0.60	0	0	0.72	0	0	0.67	-1	0	0.78	0	0	0.73	0	0	-	-	-

TABLE IV
MEAN ERROR (ME), MEAN ABSOLUTE ERROR (MAE), ROOT MEAN SQUARE ERROR (RMSE), AND COEFFICIENT OF DETERMINATION (R^2) OF THE CROWN PARAMETERS ESTIMATION RESULTS OBTAINED ON THE FUSED SET OF CROWNS.

	Height (m)	**Crown Width (m)**	**90° Crown Width (m)**
ME	0.04	-0.42	0.68
MAE	0.30	1.06	1.41
RMSE	0.39	1.46	1.68
R^2	0.99	0.86	0.77

estimation of the crown volume, as proved by the high $R^2 = 0.75$ value obtained with the measured DBH.

V. CONCLUSION AND DISCUSSION

In this paper we have presented an automatic method for the fusion of ALS and TLS data to accurately reconstruct forest structure. The proposed method is suited for localized forest analysis, which aims to accurately measure especially the crown parameters at the individual tree level. The main novelty of the presented work is related to the following:

1) the use of the ALS data for the automatic registration of multiple TLS scans;

2) the efficacy of TLS crown delineation performed using the ALS segmentation results;

3) the improvement in forest structure modeling after the fusion of the ALS and TLS point clouds.

The proposed method does not require any reference target during the acquisition of the TLS scan, thus leading to efficient and practical TLS acquisition campaigns. Moreover, by

registering the ALS segmented image to the TLS scan, we accurately delineate single tree crowns present in the terrestrial data without requiring manual analysis or refinement. The registration validation strategy, based on the normalized correlation matrix, enables automatic detection of possible residual misregistration, due to potential problems related to the TLS scan acquisition.

The obtained results verify that the proposed method accurately matches the TLS and ALS data by using the spatial distribution of the trees in an open woodland forest. We furthermore concluded that the fusion of these data leads to a more comprehensive representation of the tree crowns. In particular, we determined that the 3-D structure of the crown is accurately reconstructed from the fused data. The resolution of the obtained fused data varies, depending on the number of terrestrial scans and the distance of the terrestrial scanner from a target. However, in our experiments the fusion resulted in accurate crown parameter estimation due to the use of the two complementary data sources.

As future developments of this work, we will investigate the estimation of other forest parameters from the set of fused, segmented crowns. We also intend to extend the method to forests that are characterized by different tree densities and forest structures.

REFERENCES

[1] G. G. Parker, Structure and microclimate of forest canopies. Forest canopies: A review of research on a biological frontier. San Diego: Academic Press, 1995.

[2] I. Ross, The Radiation Regime and Architecture of Plant Stands, vol. 3. Norwell, MA, USA: Dr W Junk, 1981.

[3] J. K. Agee, "The influence of forest structure on fire behavior," in Proceedings of the 17th annual forest vegetation management conference, 1996, pp. 16–18.

[4] M. A. Finney et al., FARSITE: Fire area simulator: model development and evaluation. US Department of Agriculture, Forest Service, Rocky Mountain Research Station Ogden, UT, 2004.

[5] M. D. Lowman and H. B. Rinker, Forest canopies. Academic Press, 2004.

[6] G. G. Parker, D. J. Harding, and M. L. Berger, "A portable lidar system for rapid determination of forest canopy structure," Journal of Applied Ecology, vol. 41, no. 4, pp. 755–767, 2004.

[7] B. Zeide and P. Pfeifer, "Fractal dimension is used to characterized tree crown," Forest Science, vol. 37, no. 5, pp. 1253–1265, 1991.

[8] D. Ellsworth and P. Reich, "Canopy structure and vertical patterns of photosynthesis and related leaf traits in a deciduous forest," Oecologia, vol. 96, no. 2, pp. 169–178, 1993.

[9] P. Oker-Blom, "Influence of penumbra on the distribution of direct solar radiation in a canopy of Scots pine," Photosynthetica, 1985.

[10] P. Oker-Blom et al., "Photosynthetic radiation regime and canopystructure in modeled forest stands," Acta For. Fenn., vol. 197, pp. 1–44, 1986.

[11] P. Stenberg, "Penumbra in within-shoot and between-shoot shading in conifers and its significance for photosynthesis," Ecological Modelling, vol. 77, no. 2, pp. 215–231, 1995.

[12] C. Field, "Allocating leaf nitrogen for the maximization of carbon gain: leaf age as a control on the allocation program," Oecologia, vol. 56, no. 2-3, pp. 341–347, 1983.

[13] T. J. Givnish, "Adaptation to sun and shade: a whole-plant perspective," Functional Plant Biology, vol. 15, no. 2, pp. 63–92, 1988.

[14] J. G. Henning and P. J. Radtke, "Detailed stem measurements of standing trees from ground-based scanning lidar," Forest Science, vol. 52, no. 1, pp. 67–80, 2006.

[15] A. Kangas and M. Maltamo, Eds., Forest Inventory: Methodology and Applications. Managing Forest Ecosystems, vol. 10. Dordrecht, The Netherlands: Springer, 2006.

[16] A. Kato, L. M. Moskal, P. Schiess, M. E. Swanson, D. Calhoun, and W. Stuetzle, "Capturing tree crown formation through implicit surface reconstruction using airborne lidar data," Remote Sensing of Environment, vol. 113, no. 6, pp. 1148–1162, 2009.

[17] C. G. Bachman, "Laser radar systems and techniques," Dedham, Mass., Artech House, Inc., 1979, 203 p., vol. 1.

[18] J. Lovell, D. L. Jupp, D. Culvenor, and N. Coops, "Using airborne and ground-based ranging lidar to measure canopy structure in Australian forests," Canadian Journal of Remote Sensing, vol. 29, no. 5, pp. 607–622, 2003.

[19] A. Wehr and U. Lohr, "Airborne laser scanning: an introduction and overview," ISPRS Journal of Photogrammetry and Remote Sensing, vol. 54, no. 2, pp. 68–82, 1999.

[20] J. Hyyppä, H. Hyyppä, D. Leckie, F. Gougeon, X. Yu, and M. Maltamo, "Review of methods of small-footprint airborne laser scanning for extracting forest inventory data in boreal forests," International Journal of Remote Sensing, vol. 29, no. 5, pp. 1339–1366, 2008.

[21] T. U. Kampe, B. R. Johnson, M. Kuester, and M. Keller, "NEON: the first continental-scale ecological observatory with airborne remote sensing of vegetation canopy biochemistry and structure," Journal of Applied Remote Sensing, vol. 4, no. 1, pp. 043510–043510, 2010.

[22] L. Korhonen, J. Vauhkonen, A. Virolainen, A. Hovi, and I. Korpela, "Estimation of tree crown volume from airborne lidar data using computational geometry," International journal of remote sensing, vol. 34, no. 20, pp. 7236–7248, 2013.

[23] H.-E. Andersen, S. E. Reutebuch, and G. F. Schreuder, "Bayesian object recognition for the analysis of complex forest scenes in airborne laser scanner data," International archives of photogrammetry remote sensing and spatial information sciences, vol. 34, no. 3/A, pp. 35–41, 2002.

[24] A. Persson, J. Holmgren, and U. Söderman, "Detecting and measuring individual trees using an airborne laser scanner," Photogrammetric Engineering and Remote Sensing, vol. 68, no. 9, pp. 925–932, 2002.

[25] D. Riaño, E. Chuvieco, S. Conde´s, J. González-Matesanz, and S. L.Ustin, "Generation of crown bulk density for Pinus sylvestris L. from lidar," Remote Sensing of Environment, vol. 92, no. 3, pp. 345–352, 2004.

[26] M. J. Falkowski, A. M. Smith, A. T. Hudak, P. E. Gessler, L. A. Vierling, and N. L. Crookston, "Automated estimation of individual conifer tree height and crown diameter via two-dimensional spatial wavelet analysis of lidar data," Canadian Journal of Remote Sensing, vol. 32, no. 2, pp. 153–161, 2006.

[27] B. Koch, U. Heyder, and H. Weinacker, "Detection of individual tree crowns in airborne lidar data," Photogrammetric Engineering & Remote Sensing, vol. 72, no. 4, pp. 357–363, 2006.

[28] J. Reitberger, C. Schnörr, P. Krzystek, and U. Stilla, "3D segmentation of single trees exploiting full waveform lidar data," ISPRS Journal of Photogrammetry and Remote Sensing, vol. 64, no. 6, pp. 561–574, 2009.

[29] V. F. Strîmbu and B. M. Strîmbu, "A graph-based segmentation algorithm for tree crown extraction using airborne lidar data," ISPRS Journal of Photogrammetry and Remote Sensing, vol. 104, pp. 30–43, 2015.

[30] J. Breidenbach, E. Næsset, V. Lien, T. Gobakken, and S. Solberg, "Prediction of species specific forest inventory attributes using a nonparametric semi-individual tree crown approach based on fused airborne laser scanning and multispectral data," Remote Sensing of Environment, vol. 114, no. 4, pp. 911–924, 2010.

[31] L. Chasmer, C. Hopkinson, and P. Treitz, "Assessing the three-dimensional frequency distribution of airborne and ground-based lidar data for red pine and mixed deciduous forest plots," Int Arch Photogramm Remote Sens Spat Inf Sci, vol. 36, p. 8W, 2004.

[32] C. Mallet and F. Bretar, "Full-waveform topographic lidar: State-of-theart," ISPRS Journal of photogrammetry and remote sensing, vol. 64, no. 1, pp. 1–16, 2009.

[33] J. G. Henning and P. J. Radtke, "Ground-based laser imaging for assessing three-dimensional forest canopy structure," Photogrammetric Engineering & Remote Sensing, vol. 72, no. 12, pp. 1349–1358, 2006.

[34] P. Tickle, A. Lee, R. Lucas, J. Austin, and C. Witte, "Quantifying Australian forest floristics and structure using small footprint lidar and large scale aerial photography," Forest Ecology and Management, vol. 223, no. 1, pp. 379–394, 2006.

[35] T. Hilker, M. van Leeuwen, N. C. Coops, M. A. Wulder, G. J. Newnham, D. L. Jupp, and D. S. Culvenor, "Comparing canopy metrics derived from terrestrial and airborne laser scanning in a Douglas-fir dominated forest stand," Trees, vol. 24, no. 5, pp. 819–832, 2010.

[36] M. Hauglin, V. Lien, E. Næsset, and T. Gobakken, "Geo-referencing forest field plots by co-registration of terrestrial and airborne laser

scanning data," International Journal of Remote Sensing, vol. 35, no. 9, pp. 3135–3149, 2014.

[37] F. Hosoi and K. Omasa, "Voxel-based 3-D modeling of individual trees for estimating leaf area density using high-resolution portable scanning lidar," Geoscience and Remote Sensing, IEEE Transactions on, vol. 44, no. 12, pp. 3610–3618, 2006.

[38] D. Kelbe, J. van Aardt, P. Romanczyk, and M. van Leeuwen, "Marker-free registration of forest terrestrial laser scanner data pairs with embedded confidence metrics," Geoscience and Remote Sensing, IEEE Transactions on., vol. 54, no. 7, pp. 4314–4330, 2016.

[39] Z. Kang, J. Li, L. Zhang, Q. Zhao, and S. Zlatanova, "Automatic registration of terrestrial laser scanning point clouds using panoramic reflectance images," Sensors, vol. 9, no. 4, pp. 2621–2646, 2009.

[40] P. Pingi, A. Fasano, P. Cignoni, C. Montani, and R. Scopigno, "Exploiting the scanning sequence for automatic registration of large sets of range maps," in Computer Graphics Forum, vol. 24, pp. 517–526, 2005.

[41] P. Theiler and K. Schindler, "Automatic registration of terrestrial laser scanner point clouds using natural planar surfaces," ISPRS Ann. Photogramm. Remote Sens. Spatial Inf. Sci, vol. 1, pp. 173–178, 2012.

[42] I. Stamos and M. Leordeanu, "Automated feature-based range registration of urban scenes of large scale," in Computer Vision and Pattern Recognition, Proceedings of IEEE Computer Society Conference on, vol. 2., pp. II–555, 2003.

[43] P. Thevenaz and M. Unser, "Optimization of mutual information for multiresolution image registration," Image Processing, IEEE Transactions on, vol. 9, no. 12, pp. 2083–2099, 2000.

[44] Paris, C., Valduga, D., & Bruzzone, L. A Hierarchical Approach to Three-Dimensional Segmentation of LiDAR Data at Single-Tree Level in a Multilayered Forest. IEEE Transactions on Geoscience and Remote Sensing, vol. 54, no. 7, pp. 4190-4203, 2016.

[45] L. Ene, E. Næsset, and T. Gobakken, "Single tree detection in heterogeneous boreal forests using airborne laser scanning and area-based stem number estimates," International Journal of Remote Sensing, vol. 33, no. 16, pp. 5171–5193, 2012.

[46] T. Lahivaara, A. Seppanen, J. P. Kaipio, J. Vauhkonen, L. Korhonen, T. Tokola, and M. Maltamo, "Bayesian approach to tree detection based on airborne laser scanning data," Geoscience and Remote Sensing, IEEE Transactions on, vol. 52, no. 5, pp. 2690–2699, 2014.

[47] E. Lindberg, L. Eysn, M. Hollaus, J. Holmgren, and N. Pfeifer, "Delineation of tree crowns and tree species classification from full-waveform airborne laser scanning data using 3-D ellipsoidal clustering," Selected Topics in Applied Earth Observations and Remote Sensing, IEEE Journal of, vol. 7, no. 7, pp. 3174–3181, July 2014.

[48] A. Ferraz, F. Bretar, S. Jacquemoud, G. Gonçalves, L. Pereira, M. Tomè, and P. Soares, "3-D mapping of a multi-layered Mediterranean forest using ALS data," Remote Sensing of Environment, vol. 121, pp. 210–223, 2012.

[49] Côté, J. F., Fournier, R. A., & Egli, R. An architectural model of trees to estimate forest structural attributes using terrestrial LiDAR. Environmental Modelling & Software, vol. 26, no. 6, pp. 761-777, 2011.

[50] L. Zhong; L. Cheng; H. Xu; Y. Wu; Y. Chen; M. Li, "Segmentation of Individual Trees From TLS and MLS Data," in IEEE Journal of Selected Topics in Applied Earth Observations and Remote Sensing, in press.

[51] B. Wu, B. Yu, W. Yue, S. Shu, W. Tan, C. Hu, Y. Huang, J. Wu, and H. Liu, "A voxel-based method for automated identification and morphological parameters estimation of individual street trees from mobile laser scanning data," Remote Sens., vol. 5, no. 2, pp. 584–611, Feb. 2013.

[52] Y. Lin and J. Hyyppa, "Multiecho-recording mobile laser scanning for enhancing individual tree crown reconstruction," IEEE Trans. Geosci. Remote Sens., vol. 50, no. 111, pp. 4323–4332, Nov. 2012.

[53] T. Hilker, N. C. Coops, D. S. Culvenor, G. Newnham, M. A. Wulder, C. W. Bater, and A. Siggins, "A simple technique for co-registration of terrestrial lidar observations for forestry applications," Remote Sensing Letters, vol. 3, no. 3, pp. 239–247, 2012.

[54] G. E. Christensen and H. J. Johnson, "Consistent image registration," Medical Imaging, IEEE Transactions on, vol. 20, no. 7, pp. 568–582, 2001.

[55] D. Kelbe, J. van Aardt, P. Romanczyk, M. van Leeuwen, and K. Cawse-Nicholson, "Single-scan stem reconstruction using low-resolution terrestrial laser scanner data," Selected Topics in Applied Earth Observations and Remote Sensing, IEEE Journal of, vol. 8, no. 7, pp. 3414–3427, 2015.

[56] D. Van der Zande, W. Hoet, I. Jonckheere, J. van Aardt, and P. Coppin, "Influence of measurement set-up of ground-based LiDAR for derivation of tree structure," Agricultural and Forest Meteorology, vol. 141, no. 2, pp. 147–160, 2006.

[57] D. Kelbe, J. van Aardt, P. Romanczyk, and M. van Leeuwen, "Multi-view, marker-free registration of forest terrestrial laser scanner data pairs with embedded confidence metrics," Geoscience and Remote Sensing, IEEE Transactions on., accepted, 2016.